*Progress In Electromagnetics Research M, Vol. 11, 37–52, 2010*

# RESONANT FREQUENCY ANALYSIS OF ANNULAR RING MICROSTRIP PATCH ON UNIAXIAL MEDIUM VIA HANKEL TRANSFORM DOMAIN IMMITTANCE APPROACH

**Ç. S. Gürel and E. Yazgan**

Department of Electrical and Electronics Engineering
Hacettepe University
Beytepe, Ankara 06800, Turkey

**Abstract**—In this study, resonant frequency of annular-ring microstrip patch on uniaxial medium is determined using equivalent models of the structure obtained in Hankel Transform Domain depending on TE and TM mode decomposition. For the simplification of the tensor form formulations, equivalent matrix operators are defined in cylindrical coordinates instead of the differential ones. Then, eigenvalue problem is solved by the application of the moment method and obtained resonant frequency characteristics are compared with that of the isotropic case for different anisotropy ratio values and structural parameters. Equivalent circuit models for the structure having multilayered substrates and superstrates are given in order to be used in the following studies on uniaxially anisotropic circular type microstrip patches.

## 1. INTRODUCTION

Spectral domain analysis has been found to be advantageous in the design of microstrip components such as antennas and resonators providing Green's functions in closed form [1–18]. In spectral domain analysis, by imposing the boundary conditions on the transformed field expressions, Green's functions can be determined in rectangular and cylindirical coordinates using Fourier Domain [4–6, 8, 9] or Hankel Trasform Domain formulations [2, 3, 7, 11–18]. In the case of multilayered substrates and superstrates, such a formulation process requires lengthy field derivations and application of multiple boundary conditions [9, 13]. Instead of this procedure, immitance

Corresponding author: Ç. S. Gürel (cigdem@hacettepe.edu.tr).

approach has been preferred in Fourier Transform Domain as presented by Itoh [1]. Depending on this formulation, various rectangular type microstrip structures are analyzed in literature without a need to the detailed formulations [9, 14]. This is due to the recursive nature of the equivalent models which can be easily extended to the multilayered case using impedance transformation equations of transmission lines. Similar to the Fourier Domain analysis of rectangular patch type structures, Hankel Transform Domain analysis of circular disc microstrip antenna with isotropic substrate is firstly presented in the study of Araki and Itoh [2]. Then, equivalent models in Hankel Transform Domain are developed and used for the analysis of a circular type isotropic structure with parasitic elements [7].

In later studies on microstrip structures, anisotropic materials, especially the uniaxially anisotropic ones have been considered due to their advantages [13–18]. It is known that some metamaterials exhibit uniaxial type anisotropy both in permittivity and permeability tensors [19]. In the following designs of rectangular and circular type microstrips, metamaterials and other uniaxially anisotropic substrates will have been used to obtain special operational characteristics. Annular-ring microstrip as another important type of circularly symmetric type microstrip patch has been preferred in the design of various microwave components, in the measurement of permittivity values of unknown dielectric substrates and in medical hyperthermia applications in its isotropic form [10–12]. These structures are also designed using uniaxially anisotropic materials and analyzed in spectral domain [14, 17, 18]. In some recent studies, new designs of annular ring microstrip structure for different purposes are also presented [20, 21].

In the analysis of circular type microstrip structures on anisotropic substrates, Hertz vector formulation in Hankel Transform Domain has been preferred in later studies [15, 16]. Hertz vector formulation in the same domain has later been used for double substrate, uniaxially anisotropic annular ring microstrip antenna by Vasconcelos et al. [17]. Then in a recent study, superconducting annular ring microstrip antenna on a uniaxially anisotropic media is analyzed using lengthy field formulations in spectral domain [18]. In those studies, formulations are complicated even in the case of single layered substrate. Simpler formulation depending on immitance approach in Hankel Transform Domain has not been given in literature for the analyses of annular ring microstrip patch on uniaxial microstrip structure. In the present study, instead of using general spectral domain immitance approach in rectangular coordinate system [1], complicated and lenghty formulations for circular patch [15, 16] and

for annular ring patch [17, 18], analysis of a microstrip circular ring structure on uniaxial medium is performed by using equivalent circuits determined based on the Hankel-transform-domain formulations. In order to simplfy the lengthy field derivations in determining the TE and TM equivalent models, equivalent matrix operators for cylindrical coordinates are presented and used similar to the Fourier domain equivalent matrix operators defined by Chen and Beker [22]. By using matrix operators instead of the differential ones, formulations in tensor form are simplified. It is shown that by properly combining the field expressions, mode decomposition is achieved and equivalent circuits according to the immitance approach in Hankel Transform domain are seperately obtained for TE and TM modes. Then, equivalent circuits are generalised for multilayered substrates and superstrates case. Formulations are validated by comparing the resulting Green's functions with that of the isotropic case when anisotropy ratio is taken as $A = 1$. Resonant frequency characteristics of the annular ring microstrip structure on uniaxial medium are then obtained using moment method and presented as the function of anisotropy ratio value and structural parameters.

## 2. THEORY

Annular-ring microstrip patch on uniaxially anisotropic medium with the optical axis is chosen as the symmetry axis is shown in Fig. 1.

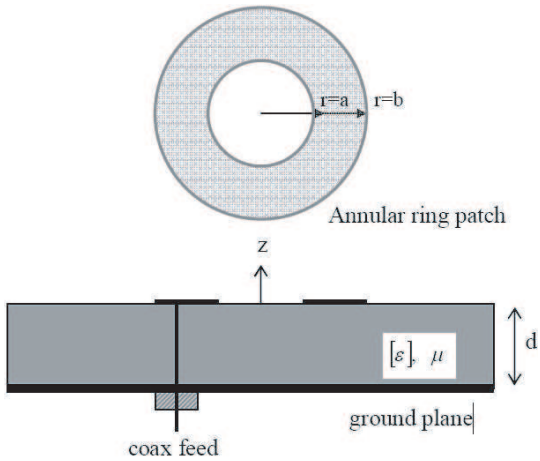


**Figure 1.** Microstrip ring structure on uniaxially anisotropic medium.

Permittivity tensor of the substrate is

$$[\varepsilon] = \begin{bmatrix} \varepsilon_r & 0 & 0 \\ 0 & \varepsilon_\phi & 0 \\ 0 & 0 & \varepsilon_z \end{bmatrix} = \varepsilon_0 \begin{bmatrix} \varepsilon_{r2} & 0 & 0 \\ 0 & \varepsilon_{r2} & 0 \\ 0 & 0 & \varepsilon_{r1} \end{bmatrix} \tag{1}$$

where $z$ is the optical axis.

In order to decompose the field expressions in the form of $TE_z$ and $TM_z$ modes, Hertz vectors are defined in the direction of optical axis [17] as

$$\bar{\Pi}_e = \Pi_e \hat{a}_z \tag{2}$$

$$\bar{\Pi}_h = \Pi_h \hat{a}_z \tag{3}$$

with their Hankel Transforms satisfying the wave equations in the form

$$\frac{\partial^2 \tilde{\Pi}_e(\alpha, z)}{\partial z^2} + \gamma_{e1,0}^2 \tilde{\Pi}_e(\alpha, z) = 0 \tag{4}$$

$$\frac{\partial^2 \tilde{\Pi}_h(\alpha, z)}{\partial z^2} + \gamma_{h1,0}^2 \tilde{\Pi}_h(\alpha, z) = 0 \tag{5}$$

where $\gamma_{e1,0}$, $\gamma_{h1,0}$ are the propagation constants along the $z$ direction in substrate and in air regions, respectively and $\alpha$ is the radial wave number.

Hankel Transform pair is defined [2] as

$$\tilde{\psi}(\alpha, z) = \int_0^\infty \psi(r, z) J_n(\alpha) r dr \tag{6}$$

$$\psi(r, z) = \int_0^\infty \tilde{\psi}(\alpha, z) J_n(\alpha, r) \alpha d\alpha \tag{7}$$

Solutions of (4), (5) for substrate region ($0 < z \leq d$) are in the form

$$\tilde{\Pi}_{h1}(\alpha, z) = (A_{h1}(\alpha) \sin \gamma_{h1} z + B_{h1}(\alpha) \cos \gamma_{h1} z) \tag{8}$$

$$\tilde{\Pi}_{e1}(\alpha, z) = (A_{e1}(\alpha) \sin \gamma_{e1} z + B_{e1}(\alpha) \cos \gamma_{e1} z) \tag{9}$$

where $\gamma_{e1}^2 = \frac{\varepsilon_{r2}}{\varepsilon_{r1}}(\omega^2 \mu_o \varepsilon_o \varepsilon_{r1} - \alpha^2)$, $\gamma_{h1}^2 = (\omega^2 \mu_o \varepsilon_o \varepsilon_{r2} - \alpha^2)$.

Similarly for the air region ($\varepsilon_{r1} = \varepsilon_{r2} = 1$, $z > d$)

$$\tilde{\Pi}_{ho}(\alpha, z) = A_{ho}(\alpha) e^{-j\gamma_{ho}(z-d)} \tag{10}$$

$$\tilde{\Pi}_{eo}(\alpha, z) = B_{eo}(\alpha) e^{-j\gamma_{eo}(z-d)} \tag{11}$$

where $\gamma_{eo}^2 = \gamma_{ho}^2 = (\omega^2 \mu_o \varepsilon_o - \alpha^2)$.

Total electric and magnetic field expressions are expressed [9] as

$$\bar{H} = j\omega\varepsilon_o \nabla \times \bar{\Pi}_e + \nabla\left(\nabla \cdot \bar{\Pi}_h\right) + \omega^2 \mu_o \varepsilon_o \varepsilon_{r2} \bar{\Pi}_h \tag{12}$$

$$\bar{E} = \omega^2 \mu_o \varepsilon_o \bar{\Pi}_e + \frac{1}{\varepsilon_{r2}} \nabla\left(\nabla \cdot \bar{\Pi}_e\right) - j\omega\mu_o \nabla \times \bar{\Pi}_h \tag{13}$$

To simplify the solution of (12) and (13), instead of using conventional vector operators, equivalent matrix operators are defined for cylindrical coordinates in Table 1, similar to the equivalent matrix operators in Fourier domain [22]. By considering azimuthal symmetry, $e^{jn\phi}$ type field variation is assumed and $\partial/\partial\phi = jn$ is taken.

Then, by starting with (12) and using matrix operators in Table 1

$$H_r = -\omega\varepsilon_o \frac{n}{r} \Pi_e + \frac{\partial}{\partial r}\frac{\partial}{\partial z} \Pi_h \tag{14}$$

$$H_\phi = -j\omega\varepsilon_o \frac{\partial}{\partial r} \Pi_e + \frac{jn}{r}\frac{\partial}{\partial z} \Pi_h \tag{15}$$

$$H_z = \left(\omega^2 \mu_o \varepsilon_o \varepsilon_{r2} - \frac{\partial^2}{\partial z^2}\right) \Pi_h \tag{16}$$

And similarly by starting with (13) and using matrix operators in Table 1

$$E_r = \frac{1}{\varepsilon_{r2}} \frac{\partial}{\partial r}\frac{\partial}{\partial z} \Pi_e + \omega\mu_o n \Pi_h \tag{17}$$

$$E_\phi = \frac{1}{\varepsilon_{r2}} \frac{jn}{r}\frac{\partial}{\partial z} \Pi_e + j\omega\mu_o \frac{\partial}{\partial r} \Pi_h \tag{18}$$

$$E_z = \left(\omega^2 \mu_o \varepsilon_o - \frac{1}{\varepsilon_{r2}} \frac{\partial^2}{\partial z^2}\right) \Pi_e \tag{19}$$

**Table 1.** Equivalent matrix operators used in cylindrical coordinates.

| | *Cylindrical vector operators* | *Equivalent matrix operators* |
|---|---|---|
| $\bar{F}$ | $(F_r \hat{a}_r + F_\phi \hat{a}_\phi + F_z \hat{a}_z)$ | $[F_r, F_\phi, F_z]^T$ |
| $\nabla\psi$ | $\left(\frac{\partial}{\partial r}\hat{r} + \frac{jn}{r}\hat{\phi} + \frac{\partial}{\partial z}F_z\right)$ | $[\frac{\partial}{\partial r}, \frac{jn}{r}, \frac{\partial}{\partial z}]^T$ |
| $\nabla\cdot\bar{F}$ | $\left(\frac{1}{r}\frac{\partial}{\partial r} r F_r + \frac{jn}{r}F_\phi + \frac{\partial}{\partial z}F_z\right)$ | $[\frac{1}{r}\frac{\partial}{\partial r} r, \frac{jn}{r}, \frac{\partial}{\partial z}][F_r, F_\phi, F_z]^T$ |
| $\nabla\times\bar{F}$ | $\frac{1}{r}\begin{vmatrix} \hat{r} & r\hat{\phi} & \hat{z} \\ \frac{\partial}{\partial r} & jn & \frac{\partial}{\partial z} \\ F_r & F_\phi & F_z \end{vmatrix}$ | $\begin{bmatrix} 0 & -\frac{\partial}{\partial z} & \frac{jn}{r} \\ \frac{\partial}{\partial z} & 0 & -\frac{\partial}{\partial r} \\ -\frac{jn}{r} & \frac{1}{r}\frac{\partial}{\partial r} r & 0 \end{bmatrix} \begin{bmatrix} F_r \\ F_\phi \\ F_z \end{bmatrix}$ |
| $\nabla^2\psi$ | $\left(\frac{1}{r}\frac{\partial}{\partial r}(r\frac{\partial}{\partial r}) - \frac{n^2}{r^2} + \frac{\partial^2}{\partial z^2}\right)\psi$ | $[\frac{1}{r}\frac{\partial}{\partial r}, \frac{-jn}{r}, -\frac{\partial}{\partial z}][r\frac{\partial}{\partial r}, \frac{-jn}{r}, \frac{-\partial}{\partial z}]^T\psi$ |

can be obtained. Hertz vectors for substrate and air regions in (8)–(11) can be expressed in the form of inverse Hankel Transform as

$$\Pi_{h1}(\alpha, z) = \int_0^\infty (A_{h1}(\alpha)\sin\gamma_{h1}z + B_{h1}(\alpha)\cos\gamma_{h1}z)J_n(\alpha r)\alpha d\alpha \quad (20)$$

$$\Pi_{e1}(\alpha, z) = \int_0^\infty (A_{e1}(\alpha)\sin\gamma_{e1}z + B_{e1}(\alpha)\cos\gamma_{e1}z)J_n(\alpha r)\alpha d\alpha \quad (21)$$

$$\Pi_{ho}(\alpha, z) = \int_0^\infty A_{ho}(\alpha)(\alpha)e^{-j\gamma_{ho}(z-d)}J_n(\alpha r)\alpha d\alpha \quad (22)$$

$$\Pi_{eo}(\alpha, z) = \int_0^\infty B_{eo}(\alpha)(\alpha)e^{-j\gamma_{eo}(z-d)}J_n(\alpha r)\alpha d\alpha \quad (23)$$

Field expressions in (14)–(16) and (17)–(19) can be written using (20)–(23) in terms of Hankel Transform by using the Bessel function identities and then decomposed in the form of $TE_z$ and $TM_z$ modes by using electric or magnetic field coefficients. For this purpose, field components and current density expressions are expressed as

$$H_\pm, E_\pm(r) = H_r, E_r(r) \pm jH_\phi, E_\phi(r) \quad (24)$$

$$J_\pm(r) = J_r(r) \pm jJ_\phi(r) \quad (25)$$

By this way, it is possible to define Green's impedance functions in Hankel Transform Domain in the form

$$\begin{bmatrix} \tilde{E}_+(\alpha) \\ \tilde{\mathrm{E}}_-(\alpha) \end{bmatrix} = \begin{bmatrix} Z_{++}(\alpha) & Z_{+-}(\alpha) \\ Z_{-+}(\alpha) & Z_{--}(\alpha) \end{bmatrix} \begin{bmatrix} \tilde{J}_+(\alpha) \\ \tilde{J}_-(\alpha) \end{bmatrix} \quad (26)$$

Hankel Transforms of (24), (25) are then organised as

$$\tilde{H}, \tilde{E} \begin{pmatrix} e \\ h \end{pmatrix}(\alpha) = \tilde{H}_+, \tilde{E}_+(\alpha) \pm \tilde{H}_-, \tilde{E}_-(\alpha) \quad (27)$$

$$\tilde{J} \begin{pmatrix} \mathrm{e} \\ \mathrm{h} \end{pmatrix}(\alpha) = \tilde{J}_+(\alpha) \pm \tilde{J}_-(\alpha) \quad (28)$$

where $\tilde{F}_{(\pm)}(\alpha)$ is in the form

$$\tilde{F}_{(\pm)}(\alpha) = \int_0^\infty F(r)J_{n\pm1}(\alpha, r)rdr \quad (29)$$

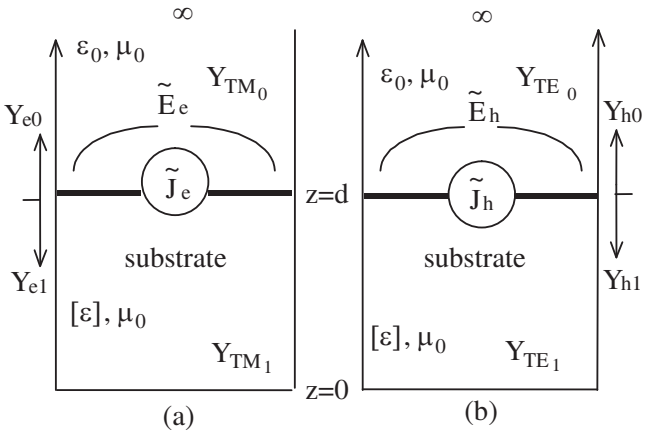


**Figure 2.** Equivalent transmission line models in Hankel Transform domain due to TE and TM modes decomposition.

This makes it possible to express field expressions seperately for each modes case in terms of single Bessel function of the form $J_{n\pm1}(\alpha, r)$ and thus in the form of Hankel transform in (29) as similarly given in [15] for circular disk structure. So, it is possible to separately determine equivalent transmission line models for $TE_z$ and $TM_z$ cases as shown in Fig. 2.

In this figure, characteristic impedances for uniaxially anisotropic medium are defined as [9]

$$Y_{TM_1} = -\frac{H_{r1}}{E_{\phi 1}} = \frac{\omega\varepsilon_0\varepsilon_{r2}}{\gamma_{e1}} \tag{30}$$

$$Y_{TE_1} = \frac{H_{\phi 1}}{E_{r1}} = \frac{\gamma_{h1}}{\omega\mu_0} \tag{31}$$

and for the air region as

$$Y_{TM_o} = -\frac{H_{r0}}{E_{\phi 0}} = \frac{\omega\varepsilon_0}{\gamma_{e0}} \tag{32}$$

$$Y_{TE_o} = \frac{H_{\phi 0}}{E_{r0}} = \frac{\gamma_{h0}}{\omega\mu_0} \tag{33}$$

Propagation constants $\gamma_{e0}$, $\gamma_{e1}$ and $\gamma_{h0}$, $\gamma_{h1}$ corresponding to $TE_z$ and $TM_z$ modes, in air and substrate regions, are given above. It is clear that characteristic admittance expressions in (30)–(33) reduce to that of the isotropic case if propagation constants are taken equal to each other as $\gamma_{e1} = \gamma_{h1} = \gamma$. Then Green's functions

of the structure can be easily determined by applying impedance or admittance transformation equations on the equivalent models in Fig. 2.

Input admittance expressions while looking downward and upward from the patch surface can be written as

$$Y_{e1} = -jY_{TM_1}\cot\gamma_{e1}d \tag{34}$$

$$Y_{h1} = -jY_{TE_1}\cot\gamma_{h1}d \tag{35}$$

and

$$Y_{e0} = Y_{TM0} \tag{36}$$

$$Y_{ho} = Y_{TE0} \tag{37}$$

where, $Z(\omega)$ matrix elements can be obtained by using the total admittance expressions of the transmission line models given above as

$$\tilde{E}_e = -Z_e\tilde{J}_e = -\frac{1}{(Y_{e1}+Y_{e0})}\tilde{J}_e \tag{38}$$

$$\tilde{E}_h = -Z_h\tilde{J}_h = -\frac{1}{(Y_{h1}+Y_{h0})}\tilde{J}_h \tag{39}$$

Then, Green's impedance functions are obtained from

$$Z_{++} = Z_{--} = \frac{Z_e + Z_h}{2} \tag{40}$$

$$Z_{+-} = Z_{-+} = \frac{Z_e - Z_h}{2} \tag{41}$$

where

$$Z_{++} = \frac{\omega\mu_0}{\gamma_0 - j\gamma_{e1}\cot(\gamma_{e1}d)} - \frac{\gamma_{h1}\mu_0}{\omega\varepsilon_0 - j\omega\varepsilon_0\varepsilon_{r2}\cot(\gamma_{h1}d)} \tag{42}$$

$$Z_{+-} = \frac{\omega\mu_0}{\gamma_0 - j\gamma_{e1}\cot(\gamma_{e1}d)} + \frac{\gamma_{h1}\mu_0}{\omega\varepsilon_0 - j\omega\varepsilon_0\varepsilon_{r2}\cot(\gamma_{h1}d)} \tag{43}$$

Equation (26) can be given in admittance form

$$\begin{bmatrix} \tilde{J}_+(\alpha) \\ \tilde{J}_-(\alpha) \end{bmatrix} = \begin{bmatrix} Y_{++}(\alpha) & Y_{+-}(\alpha) \\ Y_{-+}(\alpha) & Y_{--}(\alpha) \end{bmatrix} \begin{bmatrix} \tilde{E}_+(\alpha) \\ \tilde{\mathrm{E}}_-(\alpha) \end{bmatrix} \tag{44}$$

where Green's admittance functions are obtained by matrix inversion as

$$Y_{++}(\alpha) = Y_{--}(\alpha) = -\frac{\gamma_{h0}}{2\omega\mu_0} - \frac{\omega\varepsilon_0}{2\gamma_{e0}} + \left(\frac{jr_{h1}}{2\omega\mu_0}\cot(\gamma_{h1}d) + \frac{j\omega\varepsilon_0\varepsilon_{r2}}{2\gamma_{e1}}\cot(\gamma_{e1}d)\right) \tag{45}$$

$$Y_{+-}(\alpha) = Y_{-+}(\alpha) = -\frac{\gamma_{h0}}{2\omega\mu_0} + \frac{\omega\varepsilon_0}{2\gamma_{e0}} + \left(\frac{jr_{h1}}{2\omega\mu_0}\cot(\gamma_{h1}d) - \frac{j\omega\varepsilon_0\varepsilon_{r2}}{2\gamma_{e1}}\cot(\gamma_{e1}d)\right) \quad (46)$$

Expressions (45) and (46) reduce to that of the isotropic case when propagation constants of TE and TM modes are taken equal to each other verifying the given formulation [2]. Hankel transform domain Green's functions of the same structure having multilayered substrates and superstrates can be recursively obtained in simple manner by eliminating the need for the determination of the field expressions and application of boundary conditions in all layers. For this purpose, equivalent circuit models determined in this study can be recursively extended for multilayered case as shown in Fig. 3. In the given equivalent models, characteristic admittances for $n$th layer can be determined for TM and TE models as

$$Y_{TM_n} = \frac{\omega\varepsilon_0\varepsilon_{rn//}}{\gamma_{en}} \quad (47)$$

$$Y_{TEn} = \frac{\gamma_{hn}}{\omega\mu_0} \quad (48)$$

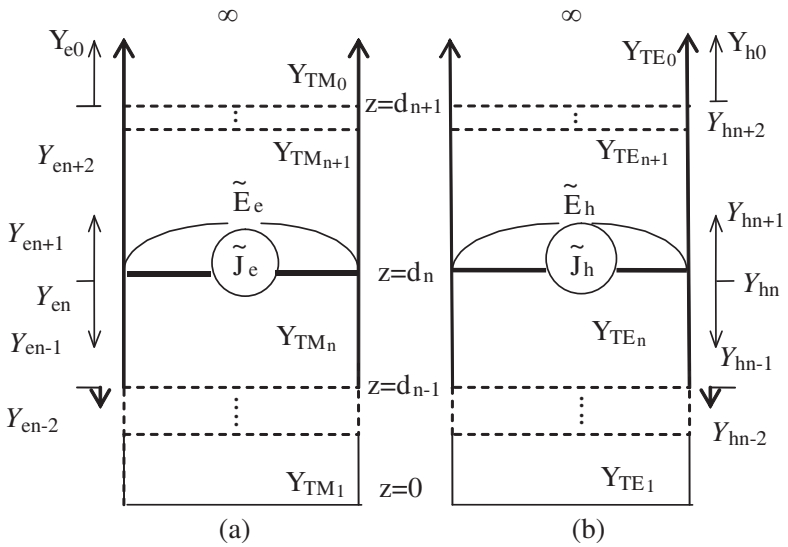


**Figure 3.** Hankel Transform Domain equivalent transmission line models for multilayered structure having uniaxial layers (a) for TM and (b) for TE modes.

and propagation constants are $\gamma_{en}^2 = \frac{\varepsilon_{rn//}}{\varepsilon_{rn\perp}}(\omega^2\mu_o\varepsilon_o\varepsilon_{rn\perp} - \alpha^2)$, $\gamma_{hn}^2 = (\omega^2\mu_o\varepsilon_o\varepsilon_{rn//} - \alpha^2)$ where $\varepsilon_{rn//}$ and $\varepsilon_{rn\perp}$ indicate the permittivity values along the non-optical and optical axes of the $n$th uniaxial layer.

Then, input impedance or admittance expressions $Z_{en}$, $Z_{hn}$ or $Y_{en}$, $Y_{hn}$ on the patch surface (i.e., at the $n$th interface) for TM and TE cases can be obtained from the impedance or admittance transformation equations of the multilayered transmission lines as

$$Y_{en} = -\frac{1}{Z_{en}} = -\frac{1}{(Y_{en+1} + Y_{en-1})} \tag{49}$$

$$Y_{hn} = -\frac{1}{Z_{hn}} = -\frac{1}{(Y_{hn+1} + Y_{hn-1})} \tag{50}$$

where

$$Y_{e,h_{n-1}} = Y_{TM,TE_n} \frac{Y_{TM,TE_n}\cos(\gamma_{e,h\,n}(d_n - d_{n-1})) + jY_{h,e_{n-2}}\sin(\gamma_{e,h\,n}(d_n - d_{n-1}))}{Y_{h,e_{n-2}}\cos(\gamma_{e,h\,n}(d_n - d_{n-1})) + jY_{TM,TE_n}\sin(\gamma_{e,h\,n}(d_n - d_{n-1}))} \tag{51}$$

and

$$Y_{e,h_{n+1}} = Y_{TM,TE_{n+1}} \frac{Y_{TM,TE_{n+1}}\cos(\gamma_{e,h\,n}(d_{n+1} - d_n)) + jY_{h,e_{n+2}}\sin(\gamma_{e,h\,n}(d_{n+1} - d_n))}{Y_{h,e_{n+2}}\cos(\gamma_{e,h\,n}(d_{n+1} - d_n)) + jY_{TM,TE_{n+1}}\sin(\gamma_{e,h\,n}(d_{n+1} - d_n))} \tag{52}$$

where other admittance expressions such as $Y_{h,e_{n\pm2}}$ can be recursively obtained.

After determining all input admittances, they can be properly combined at the patch surface as in the case of single layered substrate to obtain Green's functions of the multilayered structure in Hankel Transform Domain. Green's impedance functions of the structure can be directly obtained by inverting the admittance matrix in (44) as

$$\begin{bmatrix} \tilde{E}_+(\alpha) \\ \tilde{E}_-(\alpha) \end{bmatrix} = \begin{bmatrix} Z_{++}(\alpha) & Z_{+-}(\alpha) \\ Z_{-+}(\alpha) & Z_{--}(\alpha) \end{bmatrix} \begin{bmatrix} \tilde{J}_+(\alpha) \\ \tilde{J}_-(\alpha) \end{bmatrix} \tag{53}$$

Eigenvalues of (53) can be determined by applying the moment method of Galerkin's type by expanding the Hankel Transforms of unknown current distributions on the conducting patch in the form of series summation of the basis functions as

$$\tilde{J}_\pm(\alpha) = \sum_{m=1}^{M} C_{m\pm}\tilde{J}_{m\pm}(\alpha) \tag{54}$$

In this study, basis functions are chosen as the TM current mode functions of the circular disk cavity which have closed form Hankel

transforms [10]. The unknown $C_{m\pm}$ coefficients can be determined by substituting Hankel transforms of the basis functions $\tilde{J}_{m\pm}(\alpha)$ in (54) and taking inner products of each of them with both sides of (53) as summarized in [10]. The resulting equations can be written in the form

$$\sum_{m=1}^{M} [Z_{im}(\omega)]\ [C_{m\pm}] = 0 \quad i = 1,\ 2,\ \ldots,\ M \tag{55}$$

with the matrix elements

$$Z_{im}^{11}(\omega) \ = \ Z_{mi}^{11}(\omega) = \int_0^\infty \tilde{J}_{si+}(\alpha) Z_{++}(\alpha,\omega) \tilde{J}_{sm+}(\alpha) \alpha d\alpha \tag{56a}$$

$$Z_{im}^{12}(\omega) \ = \ Z_{mi}^{21}(\omega) = \int_0^\infty \tilde{J}_{si+}(\alpha) Z_{+-}(\alpha,\omega) \tilde{J}_{sm-}(\alpha) \alpha d\alpha \tag{56b}$$

$$Z_{im}^{22}(\omega) \ = \ Z_{mi}^{22}(\omega) = \int_0^\infty \tilde{J}_{ssi-}(\alpha) Z_{--}(\alpha,\omega) \tilde{J}_{sm-}(\alpha) \alpha d\alpha \tag{56c}$$

Then, the roots of determinant of the coefficient matrix are searched from

$$\det |Z_{ij}\ (\omega = 2\pi(f_r + jf_i))| = 0 \tag{57}$$

where resonant frequency is the real part of the solution.

## 3. NUMERICAL RESULTS

In this part, resonant frequency variation of an annular ring microstrip patch on uniaxial medium is presented. In the numerical solution of the resonant frequency as the determinant of the moment method matrix, FORTRAN programming software is used. In Fig. 4, resonant frequency versus anisotropy ratio is shown for dominant $TM_{11}$ mode operation by varying the anisotropy ratio of the substrate where anisotropy ratio is defined as $A = \varepsilon_{r2}/\varepsilon_{r1}$. In this figure, resonant frequency shift corresponding to two different normalized substrate thicknesses are shown for lossless and lossy substrate cases.

As it is seen from the figure that uniaxial anisotropy effect on the resonant frequency of ring resonator is significant and must be taken into account especially for thick substrate case. The increase or decrease in resonant frequency is the result of decrease or increase in effective permittivity due to adjustment of the substrate anisotropy ratio. Substrate losses can be ignored due to very small effect on the resonant frequency as shown by the dashed lines. In the case of

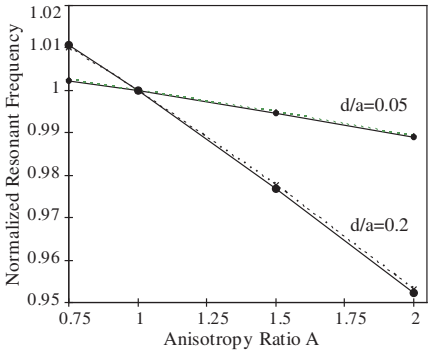


**Figure 4.** Resonant frequency versus anisotropy ratio for different normalized substrate thickness values. $a = 0.71\,\text{cm}$, $\varepsilon_{r1} = 2.43$, $b = 2a$, $\varepsilon''_{r1} = 2.43$, $\varepsilon''_{r2} = 0$ (—), $\varepsilon''_{r2} = 0.5$ (- - -).

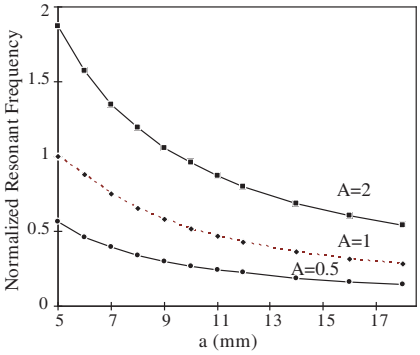


**Figure 5.** Normalized resonant frequency versus inner ring radius for different anisotropy ratio values, $\varepsilon_{r2} = 4.6$, $d = 1.2\,\text{mm}$.

high anisotropy ratio ($A = 2$), resonant frequency shift when substrate losses are considered and not considered is around 0.2% for thick substrate case ($d/a = 0.2$) and for low anisotropy ratio case ($A = 0.5$) the change in the resonant frequency is around 0.07% for thin substrate case ($d/a = 0.05$). According to the small change in resonant frequency in each case, substrate loss effect is ignored in the following parts.

In Fig. 5, resonant frequency versus inner radius of an annular ring is shown. In this figure relative permittivity value along non-optical axes are taken as $\varepsilon_{r2} = 4.6$ and substrate thickness as $d = 1.2\,\text{mm}$. It is observed in the figure that if anisotropy ratio is adjusted to a smaller value than one (i.e., smaller than isotropic case), resonant frequency decreases. Opposite is true when anisotropy ratio is greater than unity. These results indicate the main effect of the substrate anisotropy and ring radius on the resonant frequency of the annular ring microstrip patch. In Fig. 6, the variation of normalized resonant frequency with substrate thickness is shown for different anisotropy ratio values.

In this figure, each of the three cases is normalized with corresponding value at $d = 0.2\,\text{mm}$. Then anisotropy ratio is adjusted by varying $\varepsilon_{r1}$, i.e., permittivity value along the optical axis. It is observed in the figure that for the cases of $A \leq 1$, incremental shift is observed in resonant frequency while for the case of $A > 1$ decremental shift is observed. This effect becomes clear when thickness of the substrate is increased. In literature, for isotropic substrate microstrip annular ring antenna, resonant frequency shift due to

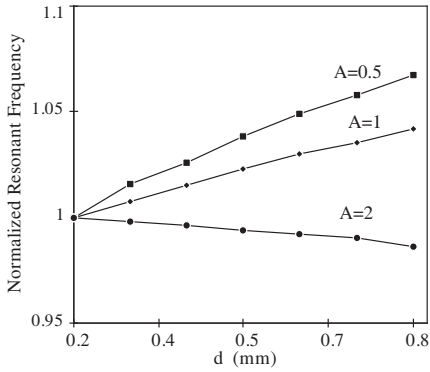


**Figure 6.** Normalized resonant frequency versus substrate thickness, for different anisotropy ratio values, $\varepsilon_{r2} = 4.6$, $b = 2a$.

increase in substrate thickness for $TM_{11}$ mode operation was previously presented in literature for isotropic substrate case and explained with the dependence of resonant frequency on the magnetic and electric field densities in near field [9].

The same situation is observed in Fig. 5, when $A = 1$ (isotropic case). For $A = 0.5$ case, similar behavior is observed. However, it is interesting to note that when anisotropy ratio is greater than one, $(A = 2)$, normalized resonant frequency behavior changes. In this case, even though resonant frequency value is greater than that of the isotropic case in magnitude, due to decreased optical axis permittivity, normalised resonant frequency starts to decrease with increasing substrate thickness. In this case, optical axis permittivity compensates the effect of near field distribution on the resonant frequency shift in $TM_{11}$ mode operation. Thus uniaxially anisotropic annular ring microstrip patch with $A > 1$ can be proposed as good resonator in this mode.

## 4. CONCLUSION

Annular ring microstrip patch on uniaxial medium is analyzed in Hankel transform domain. Equivalent circuit models in this domain are determined from field decomposition following a similar procedure with the general spectral domain immitance approach in rectangular coordinate system. In the study, resonant frequency is determined for different anisotropy ratio values and structural parameters. The results point out that uniaxial anisotropy considerably affects the resonant behavior of the structure with respect to isotropic case.

In the following studies, similar structures with circularly symmetric type patches can be designed in multilayered form with anisotropic substrates and superstrates for which Green's functions will be easily determined according to the given recursive type formulations.

## ACKNOWLEDGMENT

This work is supported by Turkish Prime Ministry State Planning Organization (DPT) and by Hacettepe University Research Foundation under contract No. 98K121710.

## REFERENCES

1. Itoh, T., "Spectral domain immitance approach for dispersion characteristics of generalised printed transmission lines," *IEEE Trans. Microwave Theory and Tech.*, Vol. 28, No. 7, 733–736, 1980.
2. Araki, K. and T. Itoh, "Hankel transform domain analysis of open circular microstrip radiating structures," *IEEE Trans. Antennas and Propagat.*, Vol. 29, No. 1, 84–89, Jan. 1981.
3. Ali, S. M., W. C. Chew, and J. A. Kong, "Vector Hankel transform analysis of annular ring microstrip antenna," *IEEE Trans. Antennas and Propagat.*, Vol. 30, No. 7, 637–644, Jul. 1982.
4. Lee, H. and V. K. Tripathi, "Spectral domain analysis of frequency dependent propagation characteristics of planar structures on uniaxial medium," *IEEE Trans. Microwave Theory and Tech.*, Vol. 30, 1188–1193, Aug. 1982.
5. Krowne, C. M., "Green's function in the spectral domain for biaxial and uniaxial anisotropic planar dielectric structures," *IEEE Trans. Antennas and Propagat.*, Vol. 32, 1273–1281, Dec. 1984.
6. Nakatani, A. and N. G. Alexopoulos, "Toward a generalised algorithm for the modeling of the dispersive properties of integrated circuit structures on anisotropic substrates," *IEEE Trans. Microwave Theory and Tech.*, Vol. 12, 1436–1441, Dec. 1985.
7. Araki, K., H. Ueda, and T. Masayuki, "Numerical analysis of circular disk microstrip antennas with parasitic elements," *IEEE Trans. Antennas and Propagat.*, Vol. 34, 1390–1394, Dec. 1986.
8. Pozar, D. M., "Radiation and scattering from a microstrip patch on a uniaxial substrate," *IEEE Trans. Antennas and Propagat.*, Vol. 35, 613–621, June 1987.

9. Nelson, R. M., D. A. Rogers, and A. G. D'Assunçao, "Resonant frequency of a rectangular microstrip patch on several uniaxial substrates," *IEEE Trans. Antennas and Propagat.*, Vol. 38, 973–981, Jul. 1990.
10. Fan, Z. and K. F. Lee, "Hankel transform domain analysis of dual-frequency stacked circular disk and annular ring microstrip antennas," *IEEE Trans. Antennas and Propagat.*, Vol. 39, No. 6, 867–870, Jun. 1991.
11. Gurel, C. S. and E. Yazgan, "Bandwidth widening in annular ring microstrip antennas with superstrate," *Proc. IEEE/AP-S Int. Symp.*, 692–695, 1995.
12. Kuo, J. T., "Vector finite Hankel transform analysis of shielded single and coupled microstrip ring structures," *IEEE Trans. Microwave Theory and Tech.*, Vol. 47, No. 11, 2161–2164, Nov. 1999.
13. Losada, V., R. R. Boix, and M. Horno, "Full wave analysis of circular microstrip resonators in multilayered media containing uniaxial anisotropic dielectrics, magnetized ferrites, and chiral materials," *IEEE Trans. Microwave Theory and Tech.*, Vol. 48, 1057–1064, Jun. 2000.
14. Barkat, W. and A. Benghalia, "Annular ring microstrip antenna in multilayered media containing uniaxial dielectrics," *First Int. Symp. on Control, Commun. and Signal Processing*, 327–330, 2004.
15. Gurel, C. S. and E. Yazgan, "Characteristics of a circular patch microstrip antenna on uniaxially anisotropic substrate," *IEEE Trans. Antennas and Propagat.*, Vol. 52, No. 10, 2532–2537, Oct. 2004.
16. Feitoza, G. M., A. G. d'Assunção, S. G. Silva, and J. R. S. Oliveira, "Analysis of circular microstrip patch antennas on anisotropic substrates using Hertz vector potentials," *Proc. 2005 Asia-Pacific Micr. Conf. (APMC2005)*, China, 2005.
17. Vasconcelos, C. F. L., S. G. Silva, M. R. M. L. Albuquerque, J. R. S. Oliveira, and G. d'Assunção, "Annular ring microstrip antennas for millimeter wave applications," *Int. J. Infrared Millim. Waves*, Vol. 28, 821–829, 2007.
18. Barkat, Q. and A. Benghalia, "Radiation and resonant frequency of superconducting annular ring microstrip antenna on uniaxial anisotropic media," *Int. J. Infrared Millim. Waves*, Jun. 2009.
19. Caloz, C. and T. Itoh, *Electromagnetic Metamaterials: Transmission Line Theory and Microwave Applications*, Wiley, 2006.

20. Rezaiesarlak, R. and F. Hodjatkashani, "Analysis of capacitively coupled microstrip-ring resonator based on spectral domain method," *Progress In Electromagnetics Research Letter*, Vol. 3, 25–33, 2008.
21. Khah, S. K., T. Chakarvarty, and P. Balamurali, "Analysis of an electromagnetically coupled microstrip ring antenna using extended feedline," *Journal of Electromagnetic Waves and Applications*, Vol. 23, No. 2–3, 369–376, 2009.
22. Chen, Y. C. and B. Beker, "Analysis of single and coupled microstrip lines on anisotropic substrates using differential matrix operators and the spectral domain method," *IEEE Trans. Microwave Theory and Tech.*, Vol. 41, 123–127, Jan. 1993.